Arabian Journal of Geosciences (2020) 13: 547
https://doi.org/10.1007/s12517-020-05531-3

ORIGINAL PAPER

# Numerical appraisal of rock mass anisotropy effect on elastic deformations of a circular tunnel

Vahid Maazallahi[1] · Abbas Majdi[1]

Received: 14 April 2019 / Accepted: 3 June 2020 / Published online: 25 June 2020


## Abstract

The paper describes effects of anisotropic mechanical properties of rock masses on elastic behaviour of a circular tunnel under both hydrostatic and non-hydrostatic in situ stress states. This study is based on field data obtained from two actual case studies. In both cases, the rock masses have transversely isotropic structures. Hence, a 2D finite element modelling based on the equivalent continuum approach is used for the analysis. The tunnel deformation behaviour has been investigated for both isotropic and transversely isotropic conditions. To evaluate the degree of anisotropy of rock mass, an "anisotropy index" and a "normalized displacement ratio" have been defined. The effect of orientation of the isotropic planes is further investigated. The results show that in a hydrostatic stress state, the maximum displacement always occurs in a direction perpendicular to the isotropic planes. In this case, three empirical equations have been developed to compute the normalized displacement ratio, the deviation, and the direction of displacement vector at any arbitrary point on the tunnel periphery. The results further show that if the anisotropy index increases, the displacement difference (the difference between the maximum and the minimum displacements) on the tunnel walls increases too. For the non-hydrostatic stress state, simultaneous effects of stress ratio, anisotropy index, and orientation of isotropic planes on normalized displacements have been investigated. In this case, the location of maximum displacement inclines towards the direction of major principal stress. This effect is more noticeable when the isotropic planes are oriented at an angle of 90° relative to the direction of the major principal stress. The paper also provides an empirical equation to determine the location of maximum displacement on the tunnel walls. Finally, the practical application of the results is further illustrated by an actual case study.

**Keywords** Equivalent continuum · Transversely isotropic · Degree of anisotropy · Elastic deformations · Displacement vector

## Introduction

Most of rocks have structural defects such as bedding planes, foliations, fracturing or joints. Presence of these defects leads to a significant change in mechanical properties in different directions, known as anisotropy. Anisotropy is observed on different scales, from small intact rock specimens to large blocks of jointed rock mass. This phenomenon plays an important role in various earthwork engineering activities such as rock slope stability (Al-Karni and Al-Shamrani 2000; Majdi and Amini 2008, 2011) and stability of underground openings (Majdi and Hassani 1989; Satici and Ünver 2015). In such cases, the differences in mechanical properties of rock strata in different directions can affect the deformation behaviour of the aforementioned rock structures.

As a customary rule for design and construction of underground openings, the existence of uniform ground conditions, i.e. homogeneity and isotropy, around the tunnels is an advantage for their permanent stability. However, the anisotropy of rocks surrounding the tunnel change the corresponding induced stresses relative to the isotropic conditions, which results in stress concentration/relaxation on the tunnel periphery. This in turn produces a non-uniform deformation on tunnel walls. Evidently, this affects the deformation behaviour of both temporary and final lining of the tunnel as well. Hence, the anisotropy has a dominant influence on deformation behaviour of an underground opening.

Responsible Editor: Murat Karakus

✉ Abbas Majdi
amajdi@ut.ac.ir

Vahid Maazallahi
v.maazallahi@ut.ac.ir

[1] School of Mining Engineering, College of Engineering, University of Tehran, Tehran 1439957131, Iran

It is apparent that recognizing the aforementioned effects is essential for a safe and economic design and construction of underground openings. Hence, in this paper, the effects of rock mass anisotropy on elastic deformations of a circular tunnel are investigated. Due to the dominant effect of the in situ stress field, analyses have been carried out in various hydrostatic and non-hydrostatic stress states. The behaviour of the rock considered in this paper is transversely isotropic. Existence of a set of structural planes, which are called "isotropic planes", is the characteristic of transversely isotropic rocks. Parallel to these planes, the deformability is the same in all directions, but they often exhibit a significantly lower deformability perpendicular to these planes than parallel to them (Wittke 2014). For the analysis, it is assumed that the longitudinal axis of the tunnel is parallel with the isotropic planes. Hence, a two-dimensional finite element modelling based on the equivalent continuum approach has been used. The tunnel wall deformations in different anisotropic situations and various stress conditions are further investigated. The results are compared with the isotropic condition, and then, the deformation changes are studied. Based on the results, some empirical relations are proposed to estimate the variations of the magnitude and the direction of the tunnel wall displacement vectors. Furthermore, the effect of rotation of the isotropic plane on tunnel wall displacement has been considered.

## A brief literature review

### Mechanical anisotropy of rocks

Anisotropy may be due to either the intrinsic nature of the rock or the extrinsic factors such as environmental effects. The primary factors are associated with the origin of the rock; in other words, the weak planes are related to rock formation processes (e.g. foliation, schistosity and cleavages). The secondary factors include existence of fractures and or sequences of different rock layers.

The rocks' anisotropy can be categorized based on the shape of the uniaxial compressive strength, $\sigma_{c\beta}$, curve relative to the angle between the weakness planes of the specimen and the maximum applied stress, $\beta$. This classification identifies two kinds of anisotropy (Ramamurthy 1993): (1) cleavage or planar and (2) bedding plane. This classification is based on three factors: maximum and minimum $\sigma_c$ at $\beta = 0°$ to 90°, and the shape of the anisotropy curve ($\sigma_{c\beta}$ vs. $\beta$). The details of this classification and the induced anisotropies are given in Table 1. Variations of $\sigma_{c\beta}$ versus β for different types of anisotropy are given in Fig. 1.

The degree of anisotropy has been introduced as an indicator for describing the anisotropy of rocks, quantitatively. Several methods are available to determine the degree of anisotropy. Ramamurthy (1993) defined an index, represented by $I_{\sigma_c}$, as the ratio of the maximum uniaxial compressive strength to the minimum uniaxial compressive strength of intact rock. Based on this index, he divides the rocks into five classes ranging from isotropic to very highly anisotropic. Franklin (1985) defined the strength anisotropy index, $I_{a(50)}$, based on the ratio of point load strength index in parallel with, $I_{a(50)\parallel}$, and perpendicular to, $I_{a(50)\perp}$, the bedding planes. Also, in 1997, an index of velocity anisotropy, *VA*, was proposed by Tsidzi based on ultrasonic wave velocity ratio in two perpendicular directions (Saroglou and Tsiambaos 2007). Saroglou et al. (2003) and Saroglou and Tsiambaos (2007) investigated the inherent anisotropy of metamorphic rocks to determine the degree of anisotropy. The current anisotropy criteria used in literatures are summarized and presented in Table 2.

## Current studies on tunnel excavation in anisotropic rocks

One of the most important problems associated with tunnelling is to determine the deformation produced during tunnel excavation. On the other hand, one of the most common assumptions that apply to majority of analytical solutions is that the ground is considered as an isotropic medium (e.g. Bobet 2002; Exadaktylos and Stavropoulou 2002; Zareifard and Fahimifar 2016). The rock surrounding the tunnel may however be anisotropic (Wang and Wang 2013). Anisotropy affects the stress distribution and deformation within the rock mass, significantly (Amadei 1996). These, in turn, affect the deformation of the tunnel, as the excavation proceeds, and the loads on lining are redistributed (Tonon and Amadei 2002). Rock mass anisotropy yields a non-uniform displacement on the tunnel wall, even though the far-field loading is hydrostatic (Bobet 2011).

There are some valuable analytical solutions to consider the influence of mechanical anisotropy of rock mass on the stability of underground structures. For example, Majdi and Hassani (1989) incorporated the in situ structural defects and strength parameters of surrounding strata in the analysis of convergence of access tunnels in longwall mining. Hefny and Lo (1999) have presented a detailed analytical solution to determine the radial and tangential displacements of a circular tunnel in an elastic transversely isotropic rock medium in which the isotropic planes are horizontal. This closed-form solution is summarized and presented in Table 3. Zhang and Sun (2011) have presented an analytical solution for a deep tunnel in a transversely isotropic rock mass with the assumption that the cross section of the tunnel is parallel with the plane of isotropy. They found that the problem in this case is the same as the isotropic case. Bobet (2011) has presented closed-form solutions for the elastic stresses and displacements of a circular tunnel excavated in a transversely isotropic rock medium. The solution has shown that the direction of the

**Table 1** Classification of types of anisotropy (The information extracted from Ramamurthy 1993; Singh and Singh 1998; Hudson and Harrison 2002)

| Type of anisotropy | | Origin | Type of structural defects | Shape and characteristics of anisotropy curve | Example |
|---|---|---|---|---|---|
| Inherent anisotropy | Bedding plane anisotropy | Sedimentary rocks | Existence of bedding planes | Shoulder type<br>Max. $\sigma_{c\beta}$ at $\beta$=0°<br>Min. $\sigma_{c\beta}$ at $\beta$=20°–40°<br>(See Fig. 1a, curve I) | Sandstone and shale |
| | Cleavage or planar anisotropy | Metamorphic and chemical rocks whose particles crystallized in specific directions | One set of cleavage | U-shaped<br>$\sigma_{c\beta}$ at $\beta$=90° is greater than $\beta$=0°<br>(See Fig. 1a, curve II) | Slates |
| | | | More than one set of cleavage | Wavy<br>$\sigma_{c\beta}$ at $\beta$=90° is greater than $\beta$=0°<br>(See Fig. 1a, curve III) | Coal, biochemical diatomite |
| Induced anisotropy | | Fractured rock masses | One set of fractures | U-shaped<br>(See Fig. 1b) | Massive igneous rock with one joint set |
| | | Fractured rock masses | More than one set of fractures | Ripple-shape<br>(See Fig. 1c) | Sedimentary layered rock with joint sets |

isotropic planes with respect to the major in situ stress is a significant parameter that affects the non-uniformity of displacements. One of the simplified assumptions in analytical solutions is circular cross section of the tunnel. Manh et al. (2014) have developed closed-form solutions for stresses and displacements around deep tunnels with arbitrary cross sections. This solution is applicable for a homogeneous, transversely isotropic and linear elastic ground with non-hydrostatic in situ stress state. Despite the development of numerous analytical methods, due to the complexity of the anisotropic effect of rock mass on behaviour of underground excavations, generally, numerical methods are frequently used to determine the distribution of stresses and displacements around the tunnels (Konietzky et al. 2001; Tonon and Amadei 2002, 2003).

In recent years, many researchers have used numerical methods to investigate the behaviour of tunnels in anisotropic and transversely isotropic rock masses. Wang et al. (2012) simulated the failure mechanism of circular tunnels in transversely isotropic rock masses by using RFPA (Realistic Failure Process Analysis) numerical code. They have investigated the 2D failure process and failure modes of tunnels in foliated rock masses. Physical model tests and numerical analysis, conducted by Zhang et al. (2012) to investigate the behaviour of stratified rock masses during underground excavations, have indicated the significant role of the dip angle of stratifications. These analyses showed that the deformations around an underground excavation increase with the dip angle of stratification. Also, the more the dip angle, the more the asymmetric distribution of deformations. Fortsakis et al. (2012) have investigated the ground response to tunnel excavation within stratified rock masses based on a two-dimensional FEM numerical analysis. They have shown the mechanism of deformations in stratified rocks and the differences between isotropic, anisotropic and transversally isotropic approaches. Kolymbas et al. (2012) analysed the behaviour of a stratified rock mass for sets of elastic constants of orthotropic and transversely isotropic media based on anisotropic linear-elastic and elasto-plastic numerical calculations. Wu and Kulatilake (2012) investigated the stability of a tunnel in a limestone rock mass using both an equivalent continuum/discontinuum model and a fully discontinuum model through three-dimensional stress analyses. This investigation on the tunnel stability under different in situ stress

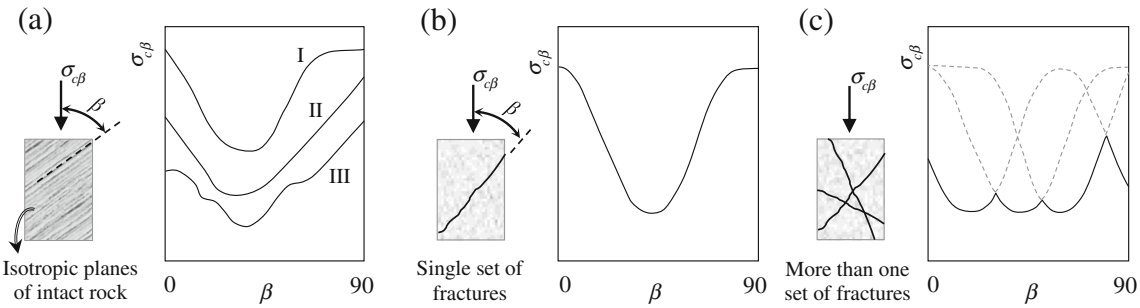


**Fig. 1** Possible variations of $\sigma_c$ versus $\beta$ for **a** intrinsic anisotropy (After Nasseri et al. 2003) and **b**, **c** induced anisotropies (Hudson and Harrison 2000)

**Table 2** The current anisotropy criteria of rocks

| Base of classification<br>Designated index<br>Reference | UCS<br>$I_{\sigma_c}$<br>(Ramamurthy 1993) | UCS<br>$I^*_{\sigma_c}$<br>(Saroglou and Tsiambaos 2007) | Point load strength<br>$Ia_{(50)}$<br>(Franklin 1985) | Ultrasonic wave velocity<br>*VA* (%)<br>By Tsidzi (Saroglou and Tsiambaos 2007) | Ultrasonic wave velocity<br>$I_{vp}$<br>(Saroglou and T siambaos 2007) |
|---|---|---|---|---|---|
| Isotropic | 1.0–1.1 | 1.0–1.1 | 1.0 | < 2.0 | – |
| Fairly anisotropic | 1.1–2.0 | 1.1–2.0 | 1.0–2.0 | 2.0–6.0 | ≤ 1.5 |
| Moderately anisotropic | 2.0–4.0 | 2.0–3.0 | | 6.0–20.0 | 1.5–2.0 |
| Highly anisotropic | 4.0–6.0 | 3.0–5.0 | 2.0–4.0 | 20.0–40.0 | > 2.0 |
| Very highly anisotropic | > 6.0 | > 5.0 | > 4.0 | > 40.0 | – |

states revealed that the maximum *x*-displacement on the tunnel rib increased with stress ratio, while the maximum *z*-displacements on the roof and floor decreased with stress ratio. A 2D semi-analytical solution has been presented by Vu et al. (2013) for stresses and displacements around a circular tunnel excavated in a transversely isotropic rock. This solution is based on the numerical integration of the equilibrium equations using the transfer matrix technique. Wang and Huang (2014) studied the joint-induced anisotropic deformation of a circular tunnel. The analysis was through a nonlinear constitutive model for a rock mass containing sets of ubiquitous joints and the associated numerical implementation which was previously developed by the same authors (Wang and Huang 2009). They concluded that the orientation and strength of joints, the tunnel overburden, and the stress ratio are the main factors affecting the deformations surrounding the tunnel. Simanjuntak et al. (2016) investigated the mechanical and hydraulic behaviour of pressure tunnels embedded in elastic transversely isotropic rocks subjected to non-hydrostatic in situ stresses by means of a 2D finite element model. It was concluded that the in situ stress ratio and the orientation of isotropic planes affect the load sharing of the

**Table 3** Closed-form solutions for determining the elastic radial and tangential displacements of the periphery of a circular tunnel in transversely-isotropic rock where the isotropic planes are horizontal (summarized after Hefny and Lo 1999)

Radial displacements:

$$u_r = \frac{R}{2(\gamma_1-\gamma_2)}\left\{P_0(\gamma_2\rho_1-\gamma_1\rho_2) + Q_0(\rho_1-\rho_2) + [P_0(\gamma_2\delta_1-\gamma_1\delta_2) + Q_0(\delta_1-\delta_2)]\cos 2\theta_p\right\}$$

Tangential displacements:

$$u_t = \frac{R}{2(\gamma_1-\gamma_2)}[P_0(\gamma_1\delta_2-\gamma_2\delta_1) + Q_0(\delta_2-\delta_1)]\sin 2\theta_p$$

where $R$ is the tunnel radius, $\theta_p$ is the angle measured from horizontal line, counter-clockwise, and the other parameters are as follows.

Hydrostatic ($P_0$) and deviatoric ($Q_0$) components of initial stress:

$$P_0 = \frac{\sigma_h+\sigma_v}{2}, \quad Q_0 = \frac{\sigma_h-\sigma_v}{2}$$

where $\sigma_h$ and $\sigma_v$ are horizontal and vertical in situ stresses, respectively.

Functions of the elastic constants:

$$\gamma_1 = \frac{\alpha_1-1}{\alpha_1+1}, \quad |\gamma_1| < 1$$
$$\gamma_2 = \frac{\alpha_2-1}{\alpha_2+1}, \quad |\gamma_2| < 1$$
$$\alpha_1^2\alpha_2^2 = \frac{S_{11}}{S_{22}}, \quad \alpha_1^2 + \alpha_2^2 = \frac{2S_{12}+S_{33}}{S_{22}}$$
$$\rho_1 = (1+\gamma_1)\beta_2 + (1-\gamma_1)\beta_1, \quad \rho_1 = (1+\gamma_2)\beta_1 + (1-\gamma_2)\beta_2$$
$$\delta_1 = (1+\gamma_1)\beta_2 - (1-\gamma_1)\beta_1, \quad \delta_1 = (1+\gamma_2)\beta_1 - (1-\gamma_2)\beta_2$$
$$\beta_1 = S_{12}-S_{22}\alpha_1^2, \qquad \beta_2 = S_{12}-S_{22}\alpha_2^2$$

Deformation coefficients related to material parameters:

$$S_{11} = \frac{1-\nu_1^2}{E_1}, \quad S_{22} = \frac{1-\nu_{12}\nu_{21}}{E_2}, \quad S_{12} = S_{21} = -\frac{\nu_{21}(1+\nu_1)}{E_2}, \quad S_{33} = \frac{1}{G_{21}}$$

in which:

$E_1$ and $E_2$ are Young's modulus in the isotropic plane and in the direction normal to the isotropic plane, respectively,

$\nu_1$ is the Poisson's ratio in the isotropic plane, $\nu_{12}$ is the Poisson's ratio for the effect of stress in the isotropic plane on the strain in the direction normal to the isotropic plane, $\nu_{21}$ is the Poisson's ratio for the effect of stress normal to the isotropic plane on the strain in the isotropic plane, and $G_{21}$ is the shear modulus normal to the isotropic plane.

Note that the following relationships among the elastic parameters must be satisfied:

$$\frac{E_2}{\nu_{21}} = \frac{E_1}{\nu_{12}}, \quad 1-\nu_1 > 0, \quad 1+\nu_1 > 0, \quad 1-\nu_1-2\nu_{12}\nu_{21} > 0$$

rock mass and the lining, significantly. Also, Schubert and Mendez (2017) presented some recommendations for excavation and support strategies based on numerical simulations and monitoring data from tunnels in foliated anisotropic rocks.

The abovementioned studies have mostly investigated the overall effects of rock mass anisotropy on the stability (including stress and deformation aspects) of tunnels. However, it would be worthy to consider the influences of the rock anisotropy on the tunnel wall's displacements as a vector quantity. Therefore, this paper has focused on variations of direction and magnitude of displacement vectors of a circular tunnel located in a transversely isotropic rock medium. Based on the outcomes of both analytical and numerical analyses, the most influencing factors affecting the ground response to tunnel excavation in transversely isotropic rocks can be listed as follows:

- The orientations of isotropic planes with respect to major principal in situ stress,
- The ratio of horizontal to vertical in situ ground stresses, $K$,
- The degree of anisotropy of rock media.

Hence, the roles of these factors are investigated by a set of numerical analysis and is represented in the following.

## Numerical analysis- input data and model construction

In this paper, the equivalent continuum approach is used to analyse the effect of rock mass anisotropy on tunnel walls' deformations. Therefore, anisotropic laboratory/field data are required to define the equivalent continuum. The required data were extracted from two actual case studies reported by Wittke (1990). The cases consist of two anisotropic jointed clay-slates with an axis of symmetry (transversely isotropic) with the equivalent parameters given in Table 4. The criteria for selection of these cases was their obvious difference in the mechanical parameters of rock mass. Therefore, this selection provides the possibility to investigate the effect of varying rock mass parameters.

To investigate the effect of different anisotropy conditions on tunnel wall deformation requires determination of the rock mass parameters for each degree of anisotropy. For this purpose, an anisotropy index, $I_E$, is defined as the ratio of the maximum to the minimum values of Young's modulus of elasticity, i.e. $I_E = E_1/E_2$. Hence, based on the data presented in Table 4, the anisotropy indices of the rock samples under present consideration will be equal to 4 and 5, respectively. Subsequently, to determine the required rock mass parameters for the desired range of anisotropy indices, the values of $E_1$ and $\nu_1$ (Poison's ratio) are taken as constants and equal to that given in Table 4. Then, with regard to $I_E = E_1/E_2$, the values of $E_2$ for different anisotropy conditions are calculated and illustrated in Fig. 2. Next, for when $I_E = 1$, the corresponding shear modulus, $G$, is calculated based on $G_{21} = G_1 = G = E/2(1+\nu)$. Furthermore, with regard to the values of $G_{21}$ in actual conditions that were given in Table 4, then the value of $G_{21}$ for each anisotropy condition can be generated by using an inverse ratio of $I_E$, based on Eq. 1 (Fig. 2).

$$G_{21} = G + \left( \frac{\frac{1}{I_E} - \frac{1}{(I_E)_{actual}}}{1 - \frac{1}{(I_E)_{actual}}} \right) \times (G - G_{actual}) \quad (1)$$

in which, $G$ is the shear modulus for isotropic condition when $I_E = 1$, and $G_{actual}$ is the shear modulus for actual condition, $(I_E)_{actual}$. Similarly, Poison's ratio, $\nu_{21}$, values are also calculated for each anisotropy condition.

To study the effect of orientation of isotropic planes, the angle from the vertical-up to the isotropic plane, measured clockwise, is called the angle of orientation and is represented by $\theta_{IP}$. Also, the location of any arbitrary point on the tunnel periphery is defined as the angle $\theta$ from the vertical-up to the considered point, measured clockwise (Fig. 3a). Next, a two-dimensional finite element program, *Phase*$^2$, has been used to analyse the numerical models for which a circular tunnel with a diameter of 5 m is assumed. So that, dimensions of the numerical models are considered 50m × 50m. The numerical model is consisted of graded 3-noded triangular elements, and its boundary conditions are depicted on Fig. 3b. The nodes on the tunnel periphery are used as the monitoring points to record the $x$- and $y$-displacements. For each case, the results of the analyses are checked with the prescribed Hefny and Lo analytical solution (Table 3) at a benchmark condition as will be shown later. Then, the established models are used for further analysis.

To account for the effect of different in situ stress fields, analyses were carried out in two different stress states: hydrostatic and non-hydrostatic. Then, to investigate the effect of different in situ stress levels, a range of 5 to 15 MPa was used for the analysis.

## Tunnel wall deformation analysis

### Analysis under hydrostatic in situ stress field

Based on Heim's hypothesis, the earth gravitational stresses, consisting of two components of vertical and horizontal, increase with depths. These components tend to equalize at high depths, which is known as hydrostatic in situ stress state (Jaeger 2009). Hence, the effects of rock mass anisotropy on magnitude and direction of displacement vectors of the tunnel wall under this stress state were investigated and presented in this section.

**Table 4** Input parameters used for numerical analysis (data extracted from Wittke 1990)

| Case | Rock type | Intact rock parameters | | | Rock mass parameters | | | | |
|---|---|---|---|---|---|---|---|---|---|
| | | $\varphi$ (deg) | $C$ (MPa) | $\sigma_t$ (MPa) | $E_1$ (MPa) | $E_2$ (MPa) | $G_{21}$ (MPa) | $\nu_1$ | $\nu_{21}$ |
| 1 | Clay slate | 28 | 7.5 | 2 | 4000 | 1000 | 480 | 0.25 | 0.06 |
| 2 | Clay slate | 30 | 10 | 1 | 10000 | 2000 | 1300 | 0.25 | 0.02 |

$\varphi$ friction angle, $C$ cohesive strength, $\sigma_t$ tensile strength, $E_1$ maximum modulus of elasticity parallel with isotropic plane, $E_2$ minimum modulus of elasticity perpendicular to isotropic plane, $G_{21}$ shear modulus perpendicular to isotropic plane, $\nu_1$ Poisson's ratio parallel with isotropic plane, $\nu_{21}$ Poisson's ratio for effect of stress normal to isotropic plane on strain in isotropic plane

## Effects of anisotropy index

In this section, to study the effect of degree of anisotropy, 9 different anisotropy indices have been used to determine the model parameters, including $I_E$ = 1, 1.25, 1.6, 2, 2.5, 3, 4, 5 and 6. Then, for each $I_E$, the model parameters have been extracted from Fig. 2 for cases 1 and 2 as was introduced before. To evaluate the effect of ground stresses, each case has been investigated under two different hydrostatic stress levels, namely, 5 and 10 MPa for case 1 and 5 and 15 MPa for case 2. Hence, 36 models have been constructed and analysed. To establish a common base of comparison, the isotropic planes are considered horizontal in all models. The tunnel wall peripheral displacements are summarized and shown in Fig. 4a–d, for $I_E$ values of 1, 2, 3, 4, 5 and 6. In this figure, the peripheral displacements of the tunnel are illustrated on a polar coordinate system. So that, the radii of each diagram denote the points on the periphery of the tunnel wall within 360°, while the concentric circles within each diagram represent the tunnel wall displacements. The peripheral displacements are measured and plotted on the diagram and forming a displacement contour. In the case of isotropic condition, the displacements are equal in all points on the tunnel walls. Therefore, the all-round displacement contour becomes a circle. However, in the case of anisotropic condition, due to non-uniform peripheral displacements, the displacement contours diverge from the circular to a bottle-neck shape. In the later condition, the non-circular displacement contour follows the degree of anisotropy. Also, in this figure, the numerical results of each case considering the actual data (Table 4) are compared with those calculated by using the closed-form solution given by Hefny and Lo (1999). For this purpose, the total displacements are calculated by the relation $D = \sqrt{u_r^2 + u_t^2}$. As can be seen from Fig. 4a–d, the numerical results for all four cases fit the analytical results, suitably, which implies the validity and the applicability of the implemented numerical approach.

Comparison of Fig. 4a with Fig. 4b, and also Fig. 4c with Fig. 4d, illustrate the effect of varying stress levels. It can be seen that the magnitudes of displacement contours for case 1 under 10 MPa stress (Fig. 4b) are 2 times the displacement contours for the case under 5 MPa stress (Fig. 4a). The same relation can be seen from Fig. 4c and d. So that, the displacement contours expand 3 times by increasing the ground stress from 5 to 15 MPa. This is in compliance with the linear elastic behaviour of the modelled rock masses. Furthermore, comparing Fig. 4a and c, which are both under a hydrostatic stress level of 5 MPa, illustrates the effect of varying rock's mechanical parameters. As it is expected, the displacements for case 2 are less than those for case 1 under the same stress level, due to its higher rock mechanical parameters (see Table 4).

To suitably evaluate the results, a "normalized displacement ratio, $D/D_i$," is defined as the ratio of the total displacement in anisotropic condition, $D$, to the total displacement in isotropic condition, $D_i$. The normalized displacement ratios have been calculated for the aforesaid cases as illustrated in

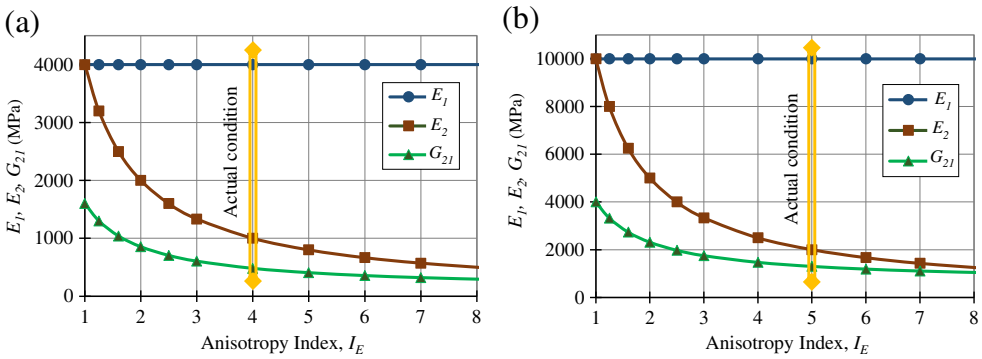


**Fig. 2** Variations of mechanical parameters of rock mass versus anisotropy index. **a** Case 1, **b** case 2

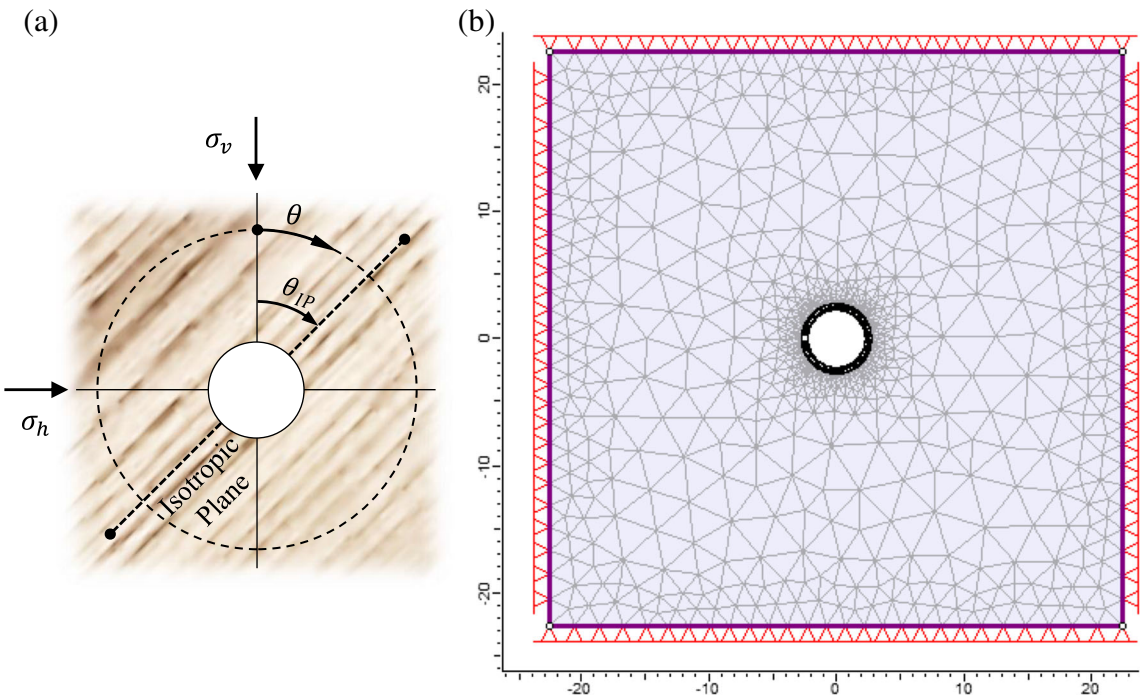


**Fig. 3** **a** Definition of orientation angle of isotropic planes, $\theta_{IP}$, and location of any arbitrary point on the tunnel periphery, $\theta$. **b** Numerical model used for the analysis

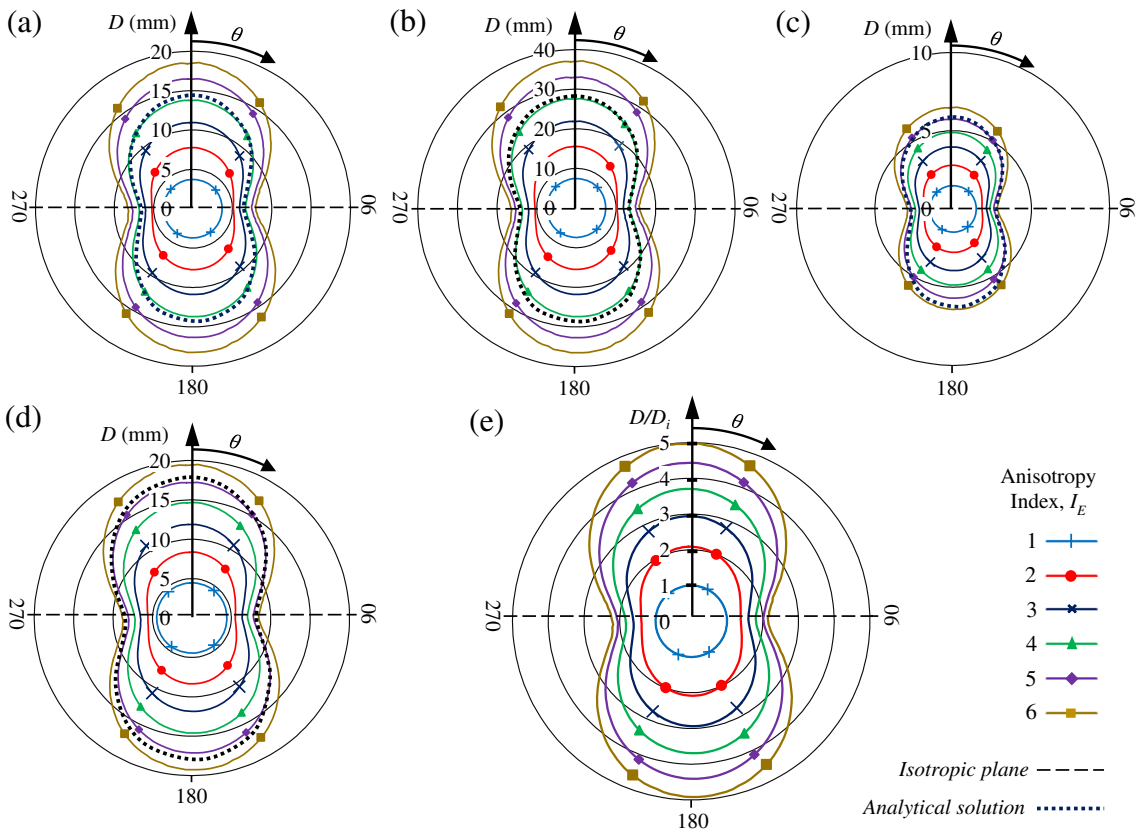


**Fig. 4** Tunnel wall displacements under different anisotropy conditions at different stress levels. **a**, **b** Case 1, under 5 and 10 MPa hydrostatic stress, respectively; **c**, **d** case 2, under 5 and 15 MPa hydrostatic stress, respectively. **e** Normalized displacements

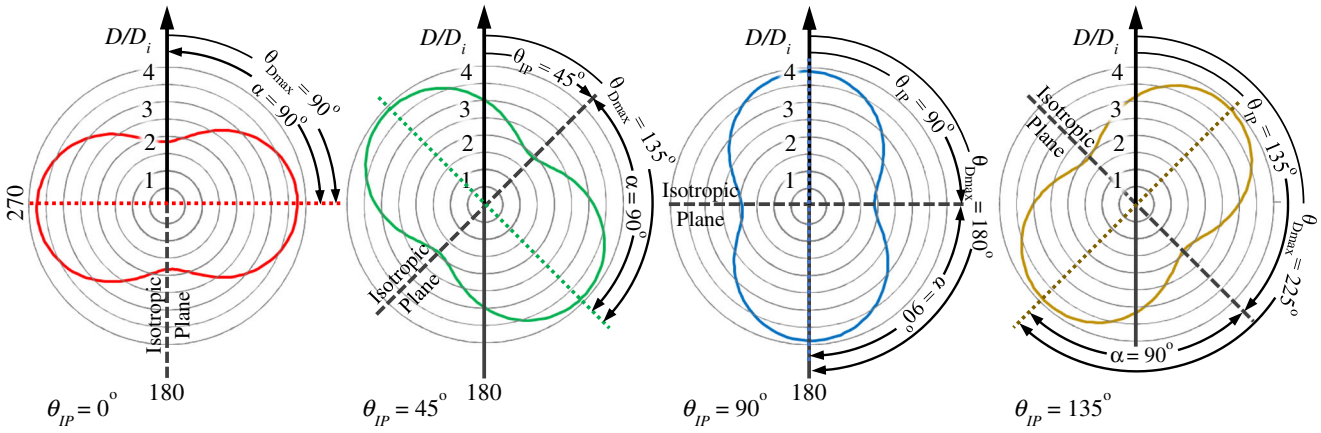


**Fig. 5** Dependency of contours of normalized displacement to the orientation of isotropic plane (in all cases $I_E = 4$)

Fig. 4e. It is noteworthy that the contours obtained for each value of the anisotropy index are the same in all investigated cases. Hence, the changes of normalized displacement ratios relative to the anisotropy index are the same in all cases irrespective to the rock's mechanical parameters and the stress levels. According to Fig. 4e, when $I_E = 6$, the maximum and the minimum displacements are 5 and 2.2 times the isotropic conditions, respectively.

## Effects of orientation of isotropic planes

To study the effects of orientation of isotropic planes on tunnel wall displacements, four models have been constructed and analysed with the isotropic planes at the angles of 0°, 45°, 90° and 135°. The rock mass parameters are taken from case 1 of Table 4, where $I_E = 4$. The normalized displacement contours in each of these orientations are shown in Fig. 5. For a quantitative characterization of the contours, the following definitions are given:

- The location of maximum displacement was defined as the angle between the vertical-up and the long axis of displacement contour, measured clockwise, and has been represented by $\theta_{Dmax}$. Actually, the maximum displacement occurs at two opposite points on the tunnel walls at $\theta_{Dmax}$ and $\theta_{Dmax} \pm 180°$.
- As well, $\alpha$ was defined as the angle between the location of maximum displacement and the isotropic plane, i.e. $\alpha = \theta_{Dmax} - \theta_{IP}$.

By the aforesaid definitions, $\alpha$ is always equal to 90° for the hydrostatic stress condition. In other words, the maximum and the minimum displacements always occur in directions perpendicular to and parallel with the isotropic planes, respectively. It is sensible to mention that the magnitudes of the displacements are equal in all cases and only the direction of the axis of the displacement contours varies (Fig. 5).

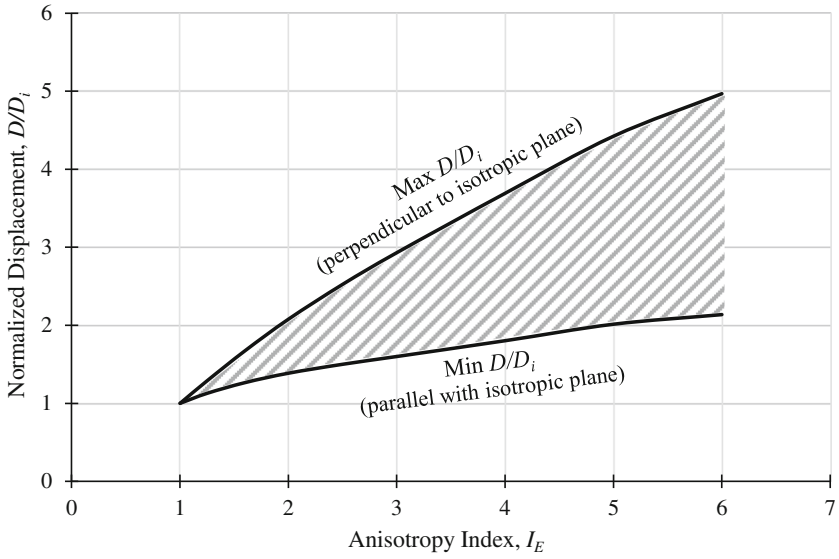


**Fig. 6** The range of tunnel walls' normalized displacements at different anisotropy indices

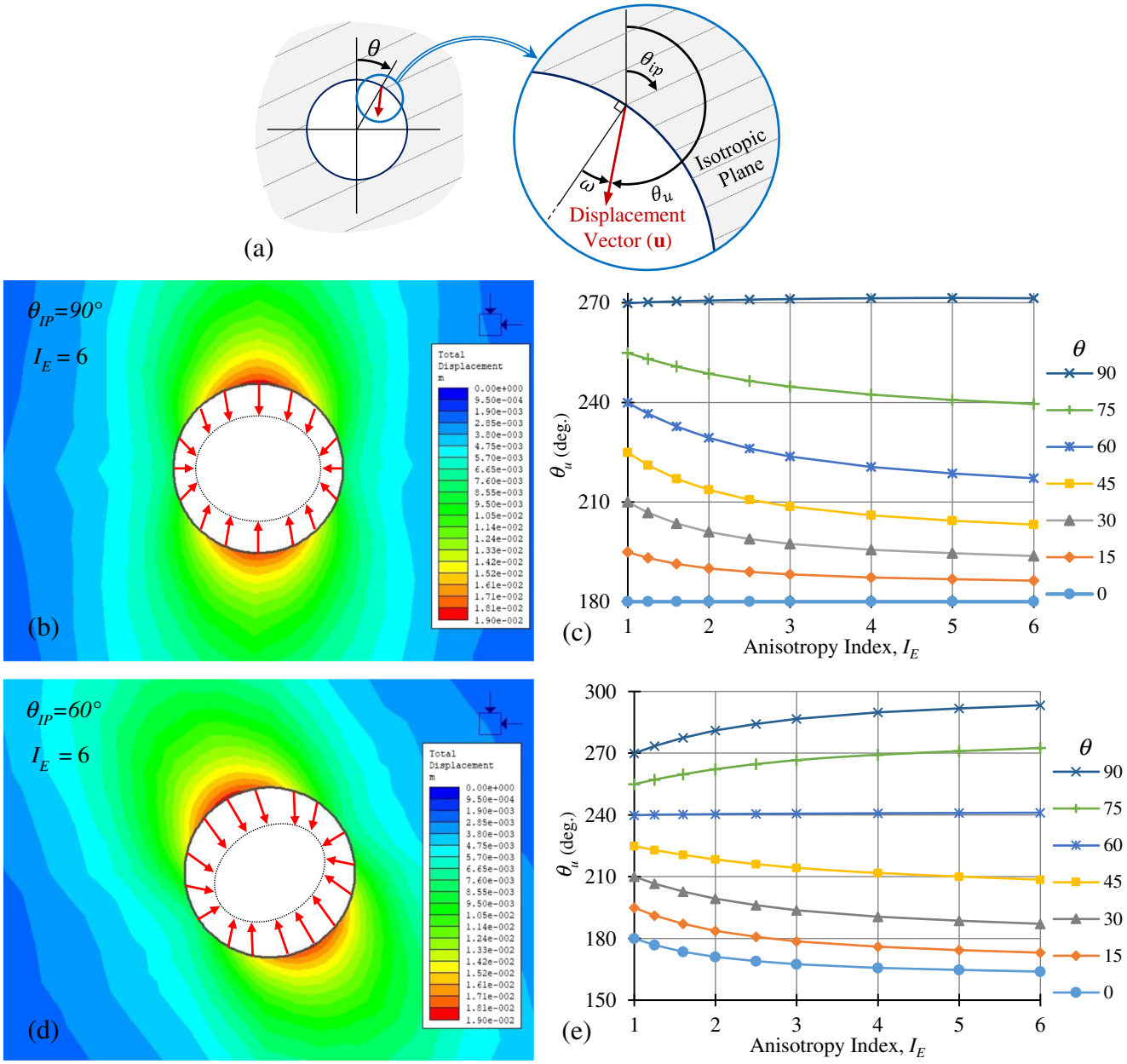


**Fig. 7** **a** Defining $\theta_u$ and $\omega$ to describe the direction and the deviation of displacement vector. **b** Tunnel walls' displacement vectors and **c** variations of its direction for case 1 (Table 4), when $\theta_{IP} = 90°$. **d** Tunnel walls' displacement vectors and **e** variations of its direction for case 1 (Table 4), when $\theta_{IP} = 60°$

### Variations of the normalized displacements

The range of variations of the normalized displacements were extracted from the results of aforementioned analyses and are depicted in Fig. 6. According to this figure, the normalized displacements are a non-linear function of the anisotropy index, so that, it can be expressed as follows:

$$1.023\, I_E^{0.4155} \le \frac{D}{D_i} \le 1.0723\, I_E^{0.888} \qquad (2)$$

It is evident that the upper and the lower bounds of Eq. 2 represent the maximum and the minimum normalized displacements, respectively. However, the upper and the lower bounds diverge as the anisotropy index increases. This is the reason for the bottle-neck shape of displacement contours. Indeed, the increase of normalized displacements relative to anisotropy index is different in various directions. So that, the difference leads to a non-uniform growth of displacements and the aforementioned shape of displacement contours, as well (Fig. 4).

### Evaluating direction of displacement vector

The tunnel wall displacement is a vector quantity whose direction, in addition to its magnitude, plays a vital role under different anisotropic conditions. It is well understood that in the case of isotropic rock mass and hydrostatic in situ stress, the displacement vector at any point on tunnel periphery is perpendicular to the tunnel wall. However, rock mass anisotropy may deviate the direction of displacement vector, significantly. Hence, in this section, the effect of rock mass anisotropy on the direction of displacement vector has been investigated. For this purpose, two parameters were defined to describe the direction of displacement vector and its deviations at any arbitrary point on the tunnel periphery (Fig. 7a):

- Direction of the displacement vector, $\theta_u$, as the angle measured from the vertical-up to the displacement vector, clockwise.
- Deviation angle of the displacement vector, $\omega$, as the angle between the normal to the tunnel wall and the displacement vector. Notice that $\omega$ is positive if measured from the normal clockwise, and negative if otherwise.

These parameters were obtained from the models executed and presented before in this paper. Additional models were built to cover the orientation of the isotropic planes from 0° to 180°. The results of numerical models for the two cases, $\theta_{IP}$ = 90° and $\theta_{IP}$ = 60°, are illustrated in Fig. 7b, d, respectively. The anisotropy indices in both cases are the same and equal to 6. It can be seen from the

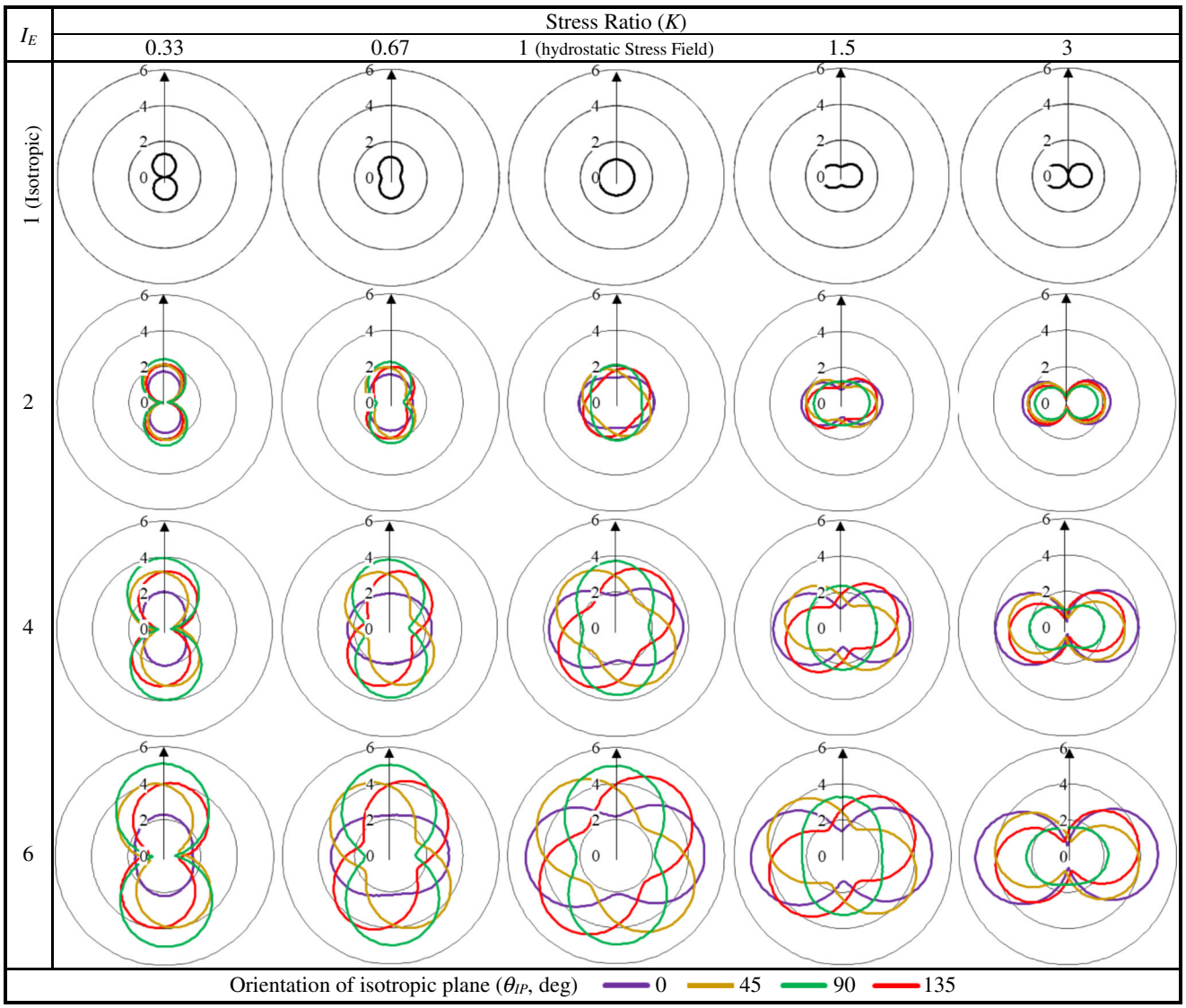


**Fig. 8** Normalized displacement, $D/D_i$, contours in different combinations of stress ratios, $K$, and anisotropy index, $I_E$, for various isotropic planes aligned at angles 0°, 45°, 90° and 135°

figures that the displacement vector is a function of orientation of the isotropic planes. For the aforementioned cases, variations of the direction of displacement vectors, $\theta_u$, versus the anisotropy index, $I_E$, for $\theta = 0°$ to $\theta = 90°$ with an interval of 15°, are illustrated in Fig. 7c, e. It can be seen that the displacement vector of the points which are located at an angle of $|\theta - \theta_{IP}| = 0°$ or 90° show no deviation, i.e. $\theta_u$ is constant and independent of $I_E$. However, the displacement vectors for the other values of $|\theta - \theta_{IP}|$ are deviated towards the direction perpendicular to the isotropic plane.

The results obtained from the abovementioned models were further analysed to calculate the deviation of the displacement vector, $\omega$, at any arbitrary point on the tunnel periphery. This led to the following relations:

*For $0° \le \theta \le 180°$:*

$$\omega = B\,\gamma\left[I_E^{-\left(501.3-0.26\gamma-0.06\gamma^2\right)/1000}-1\right] \tag{3}$$

in which

$$B = \begin{cases} +1 & \theta \le \theta_{IP} \\ -1 & \theta > \theta_{IP} \end{cases} \tag{4}$$

and

$$\gamma = \begin{cases} \theta - \theta_{IP} + 90° & \theta \le \theta_{IP} \\ \theta_{IP} - \theta + 90° & \theta > \theta_{IP} \end{cases} \tag{5}$$

*For $180° < \theta \le 360°$:*

For any point which is located within the range of $\theta$ = 180°–360°, $\omega$ can be obtained by applying an opposite sign to the value that is calculated for the angle of $\theta - 180°$ using Eq. 3.

Subsequently, the direction of the displacement vector, $\theta_u$, can be computed by using the following relationship:

$$\theta_u = \begin{matrix} \theta + \omega + 180^\circ & 0^\circ < \theta \le 180^\circ \\ \theta + \omega - 180^\circ & 180^\circ < \theta \le 360^\circ \end{matrix} \tag{6}$$

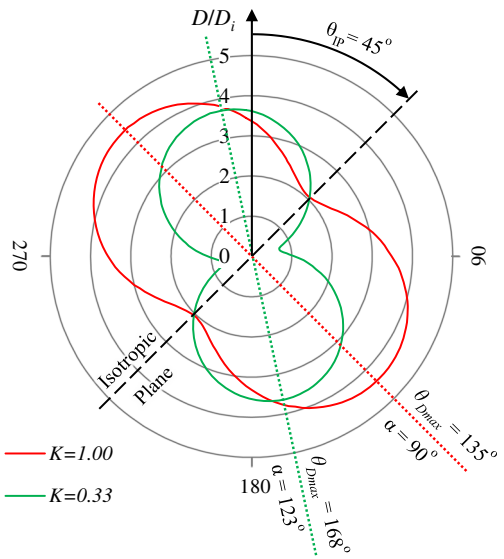


**Fig. 9** The normalized displacement, $D/D_i$, contours and the location of maximum displacement, $\theta_{Dmax}$, for the orientation of isotropic plane $\theta_{IP}$ = 45°, $I_E$ = 5, $K$ = 0.33 to $K$ = 1 and $\alpha = \theta_{Dmax} - \theta_{IP}$

## Analysis under non-hydrostatic in situ stress field

Generally, the ground stress states at low depths or under the effect of tectonic activities are non-hydrostatic. The difference in the components of ground stresses affects the deformation behaviour of underground spaces. The higher the difference in ground stresses components, the more the non-uniformity of the tunnel wall displacements. Combination of rock mass anisotropy and non-hydrostatic stress state increases the complexity of the underground structure's behaviour. Therefore, these effects are investigated in this paper and presented hereafter.

### Effects of anisotropy index

To study the effect of anisotropy index, 125 different numerical models have been constructed and analysed with anisotropy indices ranging from 1 to 7. In these models, the isotropic planes have been considered with different orientation angles: 0°, 45°, 90° and 135°. The stress ratios of 0.33, 0.67, 1, 1.5 and 3 have been applied in models. In all cases, 15 MPa was used as the maximum stress, whereas the minimum stress was calculated based on the stress ratio, $K$. The results are summarized in terms of normalized displacement, $D/D_i$, and shown in Fig. 8 for the cases of $I_E$ = 1, 2, 4 and 6.

Figure 8 illustrates the simultaneous effects of the three parameters: $K$, $I_E$, and $\theta_{IP}$ on the normalized displacements. Hence, the effect of each of these parameters can be described as follows:

- In the case of hydrostatic stress field, the shapes of the normalized displacement contours are the same for isotropic planes oriented at any angles. In this case, as the anisotropy index increases, the displacement contours, due to the displacements' increase, becomes larger.
- At any given stress ratio and degree of anisotropy, the changes in orientation of the isotropic planes cause significant changes in size and direction of the displacement contours. This change of orientation greatly affects the maximum and the minimum displacements. For example, for $K$ = 0.67 and $I_E$ = 6, the maximum normalized displacements are 3.3, 4.3 and 5.0 for the

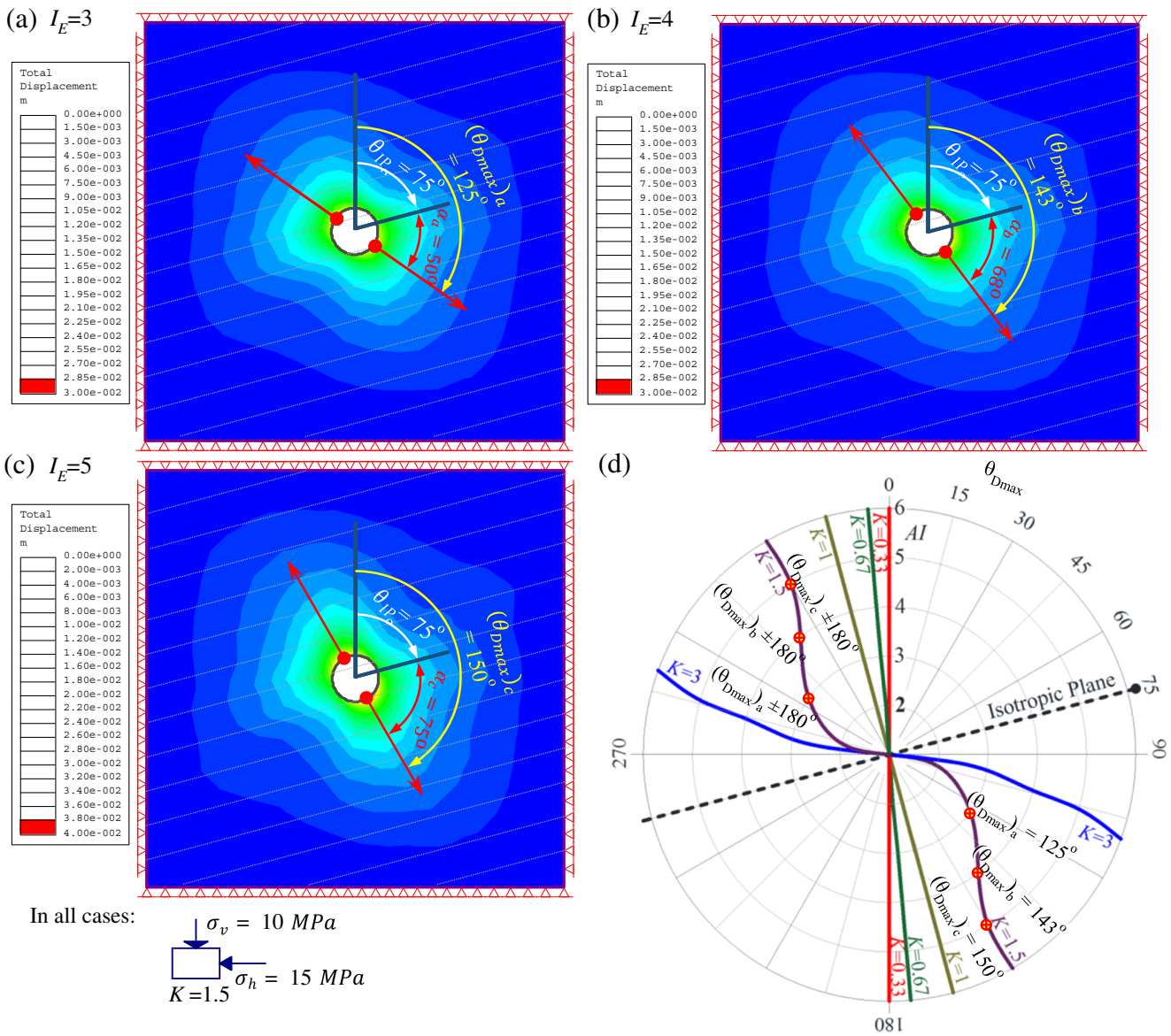


**Fig. 10** Graphical determination of the maximum displacement location on tunnel wall under three different anisotropy conditions

isotropic planes oriented at angels of 0°, 45° and 90°, respectively.

- At any given stress ratio and orientation of isotropic planes, an increase in anisotropy index will increase the size of the displacement contour. In this case, the direction of the contour does not change significantly. For example, when $K$ = 1.5 and $\theta_{IP}$ = 0°, the increase of anisotropy index from 2 to 6 increases the maximum and the minimum normalized displacements from 2.25 and 0.76 to 5.03 and 1.36, respectively.
- At any given anisotropy index and orientation of isotropic planes, the change of stress ratio affects both the size and the alignment of the displacement contours, significantly. For example, when $I_E$ = 5 and $\theta_{IP}$ = 45°, the increase of stress ratio from 0.33 to 1 changes the value and the location of the maximum normalized displacements from 3.71 to 4.45 for $\theta_{Dmax}$ = 168° to $\theta_{Dmax}$ = 135°, respectively (Fig. 9). It must be born in mind that, in all cases, $\alpha = \theta_{Dmax} - \theta_{IP}$.

Furthermore, in the case of non-hydrostatic stress field, the difference between the maximum and the minimum displacements is higher than that of the case of hydrostatic stress field. On the other hand, irrespective to the stress ratio, the normalized displacement increases with the increase of the anisotropy index. Therefore, in all, the following concluding remarks can be drawn:

- An increase in anisotropy index will increase the amount of normalized displacements, irrespective to the stress ratio, $K$.

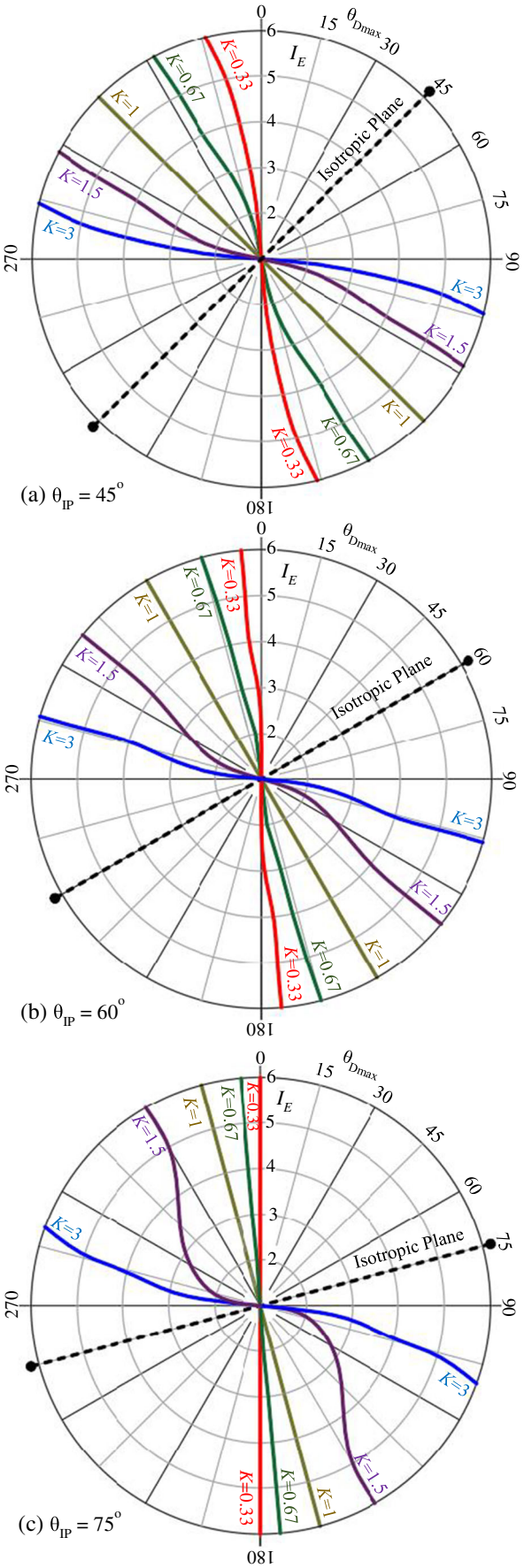


**Fig. 11** The location of maximum displacement on tunnel walls, $\theta_{Dmax}$, based on anisotropy index, $I_E$, and stress ratio, $K$, for isotropic planes oriented at **a** $\theta_{IP} = 45°$, **b** $\theta_{IP} = 60°$ and **c** $\theta_{IP} = 75$

– An increase/decrease of the stress ratio compared to the hydrostatic stress conditions leads to a larger difference between the maximum and the minimum displacements on tunnel walls.

### Effects of orientation of isotropic planes

The effects of orientation of isotropic planes on tunnel wall displacements under non-hydrostatic stress conditions are also illustrated in Fig. 8. As it can be seen, the variations of the stress ratios have significant effects on the alignment of deformation contours. In this case, an increase/decrease of the $K$ value compared to the hydrostatic stress condition increases the deviation of the displacement contours relative to the hydrostatic stress condition. Therefore, these effects are investigated by 90 further numerical models. The numerical models have been built and analysed with different combinations of stress ratios and anisotropy indices for isotropic planes oriented at $\theta_{IP} = 45°$, 60° and 75°. Based on the results of these analyses, $\alpha$ can be stated as follows:

$$\alpha = \begin{cases} (180° - \theta_{IP}) \times I_E^{0.64\,K\,(\sin\theta_{IP}-1)} & K < 1 \\ 90° & K = 1 \\ (90° - \theta_{IP}) \times I_E^{-0.43\,K*\cos(\theta_{IP})+0.86} & K > 1 \end{cases} \quad (7)$$

Then, the location of maximum displacement, $\theta_{Dmax}$, can be determined by:

$$\theta_{Dmax} = \alpha + \theta_{IP} \quad (8)$$

It must be reminded that the maximum displacement occurs on two opposite points on the tunnel wall at $\theta_{Dmax}$ and $\theta_{Dmax} \pm 180°$.

The tunnel-induced displacements in three cases of anisotropy indices under a non-hydrostatic stress field are illustrated in Fig. 10a–c. In these cases, the orientations of isotropic planes, $\theta_{IP} = 75°$. However, the anisotropy index is different for each case, so that, $I_E = 3$, 4 and 5. Then, a graphical representation is given to determining the location of maximum displacement that occurs on the tunnel walls at an angle of $\theta_{Dmax}$ as shown in the Fig. 10d diagram. In this diagram, the radial axis represents the anisotropy index, $I_E$, while the angular axis represents the location of maximum displacement on the tunnel wall, $\theta_{Dmax}$. As it can be seen, the maximum displacements for these cases occur at $\theta_{Dmax} = 125°$, 143° and 150° whose corresponding $\alpha = \theta_{Dmax} - \theta_{IP}$ are 50°, 68° and 75°. In other words, the location of maximum displacement

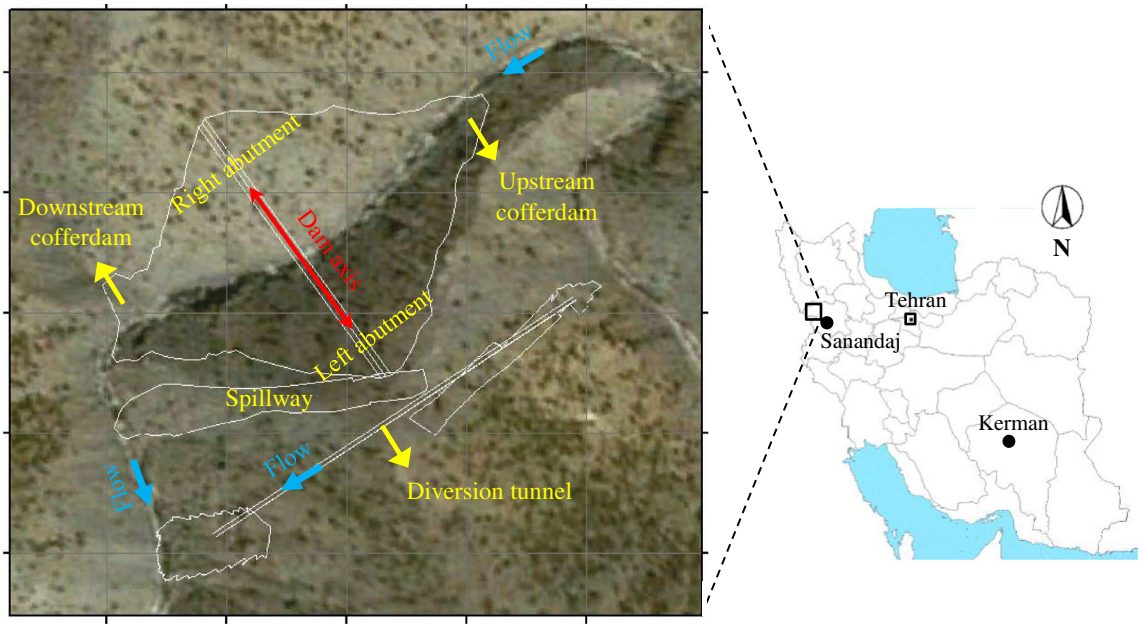


**Fig. 12** Geographical location and general layout of Kaniguizhan dam and its structures, Kurdistan, Iran

deviated 40°, 22° and 15° for the cases in Fig. 10a–c with regard to the hydrostatic stress condition, respectively.

Furthermore, three diagrams are given in Fig. 11 to demonstrate the determination of the maximum displacement location for the orientations of isotropic planes at $\theta_{IP}$ = 45°, 60° and 75°. The figure illustrates that, when the stress ratio, $K$ = 1, the location of maximum displacement is always perpendicular to the isotropic plane, as was stated in the previous sections and in Eq. 7. However, for $K \neq 1$, the location of the maximum displacement tends towards the direction of the maximum stress. So that, for $K < 1$, the location of maximum displacement tends to move towards the vertical direction, and, for $K > 1$, the location of the maximum displacement tends to move towards the horizontal direction. However, as the anisotropy index increases, these effects will diminish. So that, by increasing the anisotropy index, the tendency of the location of maximum displacement towards the maximum stress becomes less significant. Also, it can be inferred that these effects become more significant as the orientation of isotropic planes tends to an angle of 90° with the direction of maximum stress. For example, compare the curve of $K$ = 0.33 in Fig. 11a–c, where the angle between the isotropic planes and maximum in situ stress (which is vertical due to $K < 1$) are 45°, 60° and 75°, respectively. This comparison illustrates that the abovementioned tendency of the location of maximum displacement towards the direction of maximum stress becomes more significant

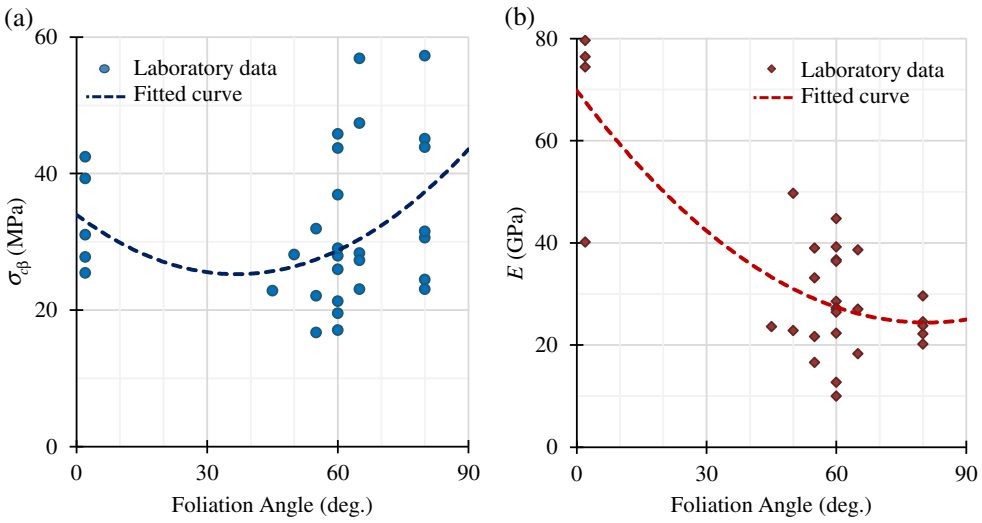


**Fig. 13** Results of laboratory tests on oriented rock samples of Kaniguizhan dam, Kurdistan, Iran. **a** Uniaxial compressive strength. **b** Young's modulus

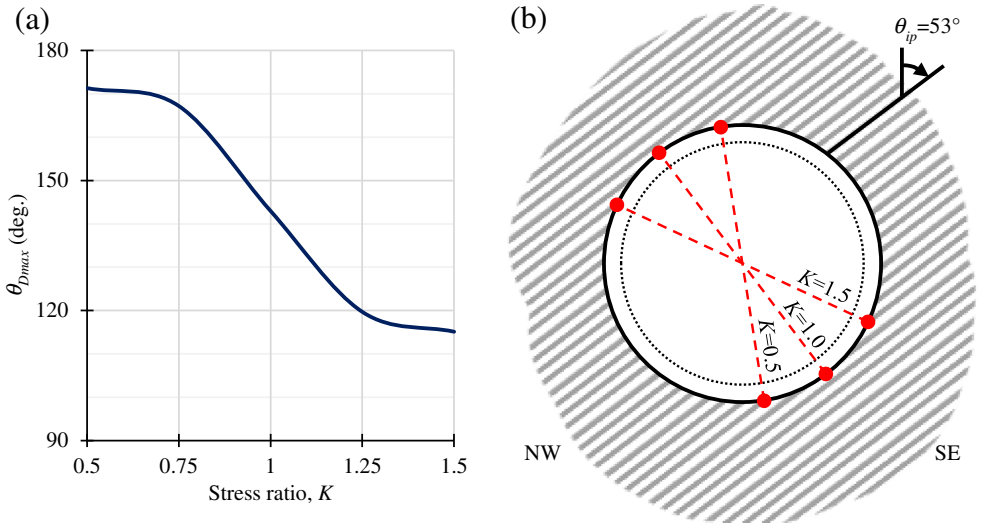


**Fig. 14** Sensitivity analysis of the location of maximum displacements against stress ratio, *K*, for the diversion tunnel of Kaniguizhan dam, Kurdistan, Iran. **a** Graph of variations. **b** Schematic representation on a cross section

when the isotropic planes are aligned at a right angle relative the maximum stress.

## Practical applications

To illustrate the practical application of the obtained formulations, an actual case study is presented in this section. The field data are taken from Kaniguizhan dam site under study to be constructed in northwest of Iran. The earth dam with a height of 122 m from the foundation will have a reservoir capacity of 133 million cubic meters. The general layout of the dam and its components is represented in Fig. 12. A wide area of the dam site is composed of Cretaceous metamorphic phyllites, which is the oldest rock unit in the dam site area. The body and reservoir of the dam, along with its related structures, are located on this rock unit. The metamorphosis processes on these phyllites resulted in forming the foliations.

The diversion tunnel of Kaniguizhan dam with a length of 485 m is located in the left abutment, where the foliations of the phyllite are oriented at a dip/dip direction of 37°/N39°W. Thus, with regard to the azimuth of the tunnel route (51° ± 180°), its longitudinal axis is almost parallel with the foliations, which are in fact the isotropic planes of the understudy rock. Therefore, the angle of orientation of isotropic planes, $\theta_{IP}$, in a cross section perpendicular to the tunnel axis is 53°. The maximum thickness of overburden on the tunnel is about 130 m. The results of laboratory uniaxial compressive strength and Young's modulus of the transversely isotropic phyllite on oriented rock samples are shown in Fig. 13. According to Fig. 13a and Table 2, this rock is categorized as 'moderately anisotropic'. Also, the curve fitted to laboratory data of Young's modulus (Fig. 13b) demonstrates that the anisotropy index, $I_E$, is equal to 3 for the understudy rock.

By means of the developed equations, a primary estimation of the state of deformations on the periphery of the tunnel has been made. To take the uncertainties into account, a sensitivity analysis has been conducted on stress ratio, *K*. Based on Eq. 2, in the case of hydrostatic stress field, the normalized displacement ratio, *D*/*Di*, is in the range of 1.61 to 2.84. This means that the displacements that occur in the direction perpendicular to the foliations ($\theta$ = 143° ± 180°) could be 1.76 times the displacements in the direction parallel with them ($\theta$ = 53° ± 180°). Also, by implementing Eqs. 5–7, the deviation of the displacement vectors, $\omega$, have been calculated. The highest deviation can be seen in the displacement vectors of the points which are located at angles of $\theta$ = 17° ± 180° and $\theta$ = 88° ± 180° on the tunnel wall. At these points, the displacement vector deviates 16° relative to the normal to the tunnel wall. Furthermore, the locations of maximum displacements for a range of *K* values from 0.5 to 1.5 were estimated by using Eqs. 7 and 8 and are shown in Fig. 14. As it can be seen, in the considered range of stress ratio, the maximum displacements may occur at angles 115°–170° (± 180°). This information can be used to provide a design guide for rock tunnel lining and monitoring design.

## Conclusion

In this paper, the anisotropic effects of rock mass on elastic behaviour of a circular tunnel have been investigated. Displacement analysis have been performed by numerical modelling of a circular tunnel under both hydrostatic and non-hydrostatic in situ stress states for different stress levels. The influences of most contributory parameters of a transversely isotropic rock medium such as anisotropy index and

the orientation of isotropic planes have been considered. In all, about 300 numerical models have been performed for the analysis. The displacements of the tunnel walls have been computed, and their contours in different conditions have been constructed in polar coordinates. The following concluding remarks have been drawn:

- Generally, the tunnel wall displacements in anisotropic media are more than the isotropic ones.
- The peripheral displacements of tunnel wall in isotropic rock mass under hydrostatic stress field are uniform, i.e. the displacement contour is circular. However, due to the change of anisotropy index and or stress ratio, the displacement contour diverges from a circular form to a bottle-neck shape.
- Though the displacement is a function of mechanical properties and stress levels, the changes of the normalized displacement ratios at any anisotropy index are the same in all cases.
- An empirical equation has been presented to estimate the normalized displacement ratio in hydrostatic stress state.
- In hydrostatic stress field, the direction of displacement vector will deviate towards the direction perpendicular to the isotropic plane. However, for the points which are located at an angle of 0° or 90° relative to the isotropic plane, the displacement vector will always be perpendicular to the tunnel wall. Also, an empirical equation has been presented to calculate the deviation and the direction of displacement vector based on the degree of anisotropy and the orientation of isotropic plane.
- In non-hydrostatic stress conditions, any change in the orientation of the isotropic planes causes a significant change in the size and direction of displacement contours. However, an increase of the anisotropy index only increases the size of the displacement contour. Furthermore, variations of the stress ratio affect both the size and the alignment of the displacement contours, significantly.
- An increase/decrease of the stress ratio with respect to the hydrostatic stress conditions leads to a larger difference between the maximum and the minimum displacements on tunnel walls. The increase of the anisotropy index has a similar impact on the displacement difference.
- Under hydrostatic stress state, the maximum and the minimum displacements always occur perpendicular to, and parallel with, the isotropic plane, respectively. However, the location of maximum displacement under non-hydrostatic stress field tends towards the maximum stress direction. This tendency becomes more significant as the orientation of isotropic planes tends towards at an angle of 90° with the direction of the maximum stress.
- An empirical equation has been presented to determine the location of maximum displacement on the tunnel walls as a function of the stress ratio, the anisotropy index and the orientation of isotropic planes.

## References


Al-Karni AA, Al-Shamrani MA (2000) Study of the effect of soil anisotropy on slope stability using method of slices. Comput Geotech 26: 83–103. https://doi.org/10.1016/S0266-352X(99)00046-4

Amadei B (1996) Importance of anisotropy when estimating and measuring in situ stresses in rock. Int J Rock Mech Min Sci Geomech Abstr 33:293–325. https://doi.org/10.1016/0148-9062(95)00062-3

Bobet A (2002) Analytical solutions for shallow tunnels in saturated ground. J Eng Mech 127:1258–1266. https://doi.org/10.1061/(asce)0733-9399(2001)127:12(1258)

Bobet A (2011) Lined circular tunnels in elastic transversely anisotropic rock at depth. Rock Mech Rock Eng 44:149–167. https://doi.org/10.1007/s00603-010-0118-1

Exadaktylos GE, Stavropoulou MC (2002) A closed-form elastic solution for stresses and displacements around tunnels. Int J Rock Mech Min Sci 39:905–916. https://doi.org/10.1016/S1365-1609(02)00079-5

Fortsakis P, Nikas K, Marinos V, Marinos P (2012) Anisotropic behaviour of stratified rock masses in tunnelling. Eng Geol 141–142:74–83. https://doi.org/10.1016/j.enggeo.2012.05.001

Franklin JA (1985) Suggested method for determining point load strength. Int J Rock Mech Min Sci Geomech Abstr 22:51–60. https://doi.org/10.1016/0148-9062(85)92327-7

Hefny AM, Lo KY (1999) Analytical solutions for stresses and displacements around tunnels driven in cross-anisotropic rocks. Int J Numer Anal Methods Geomech 23:161–177. https://doi.org/10.1002/(SICI)1096-9853(199902)23:2<161::AID-NAG963>3.0.CO;2-B

Hudson J, Harrison J (2000) Engineering rock mechanics: an introduction to the principles, 2nd edn. Elsevier Science Ltd, Oxford

Jaeger J (2009) Rock mechanics and engineering, 2nd edn. Cambridge University Press, Cambridge

Kolymbas D, Lavrikov SV, Revuzhenko AF (2012) Deformation of anisotropic rock mass in the vicinity of a long tunnel. J Min Sci 48: 962–974. https://doi.org/10.1134/S1062739148060032

Konietzky H, Te Kamp L, Hammer H, Niedermeyer S (2001) Numerical modelling of in situ stress conditions as an aid in route selection for rail tunnels in complex geological formations in South Germany. Comput Geotech 28:495–516. https://doi.org/10.1016/S0266-352X(01)00009-X

Majdi A, Amini M (2008) Effects of geostructural weaknesses on flexural toppling. In: 5th Asian Rock Mechanics Symposium (ARMS5). Tehran, Iran, pp 611–618

Majdi A, Amini M (2011) Analysis of geo-structural defects in flexural toppling failure. Int J Rock Mech Min Sci 48:175–186. https://doi.org/10.1016/j.ijrmms.2010.11.007

Majdi A, Hassani F (1989) Access tunnel convergence prediction in longwall coal mining. Int J Min Geol Eng 7:283–300. https://doi.org/10.1007/BF00896593

Manh HT, Sulem J, Subrin D (2014) A closed-form solution for tunnels with arbitrary cross section excavated in elastic anisotropic ground. Rock Mech Rock Eng 48:277–288. https://doi.org/10.1007/s00603-013-0542-0

Nasseri MHB, Rao KS, Ramamurthy T (2003) Anisotropic strength and deformation behavior of Himalayan schists. Int J Rock Mech Min Sci 40:3–23. https://doi.org/10.1016/S1365-1609(02)00103-X

Ramamurthy T (1993) Strength and modulus responses of anisotropic rocks. In: Brown ET (ed) Comprehensive rock engineering. Pergamon press, pp 313–329

Saroglou H, Tsiambaos G (2007) Classification of anisotropic rocks. In: Sousa RE (ed) 11th Congress of the International Society for Rock Mechanics. Taylor & Francis Group, Lisbon, pp 191–196

Saroglou H, Marinos P, Tsiambaos G (2003) The anisotropic nature of selected metamorphic rocks from Greece. In: ISRM 2003–Technology roadmap for rock mechanics. South African Institute of Mining and Metallurgy, pp 1019–1024

Satici O, Ünver B (2015) Assessment of tunnel portal stability at jointed rock mass: a comparative case study. Comput Geotech 64:72–82. https://doi.org/10.1016/j.compgeo.2014.11.002

Schubert W, Mendez JMD (2017) Influence of foliation orientation on tunnel behavior. Procedia Eng 191:880–885. https://doi.org/10.1016/j.proeng.2017.05.257

Simanjuntak TDYF, Marence M, Schleiss AJ, Mynett AE (2016) The interplay of in situ stress ratio and transverse isotropy in the rock mass on prestressed concrete-lined pressure tunnels. Rock Mech Rock Eng 49:4371–4392. https://doi.org/10.1007/s00603-016-1035-8

Singh KB, Singh TN (1998) Ground movements over longwall workings in the Kamptee coalfield, India. Eng Geol 50:125–139. https://doi.org/10.1016/S0013-7952(98)00005-2

Tonon F, Amadei B (2002) Effect of elastic anisotropy on tunnel wall displacements behind a tunnel face. Rock Mech Rock Eng 35:141–160. https://doi.org/10.1007/s00603-001-0019-4

Tonon F, Amadei B (2003) Stresses in anisotropic rock masses: an engineering perspective building on geological knowledge. Int J Rock Mech Min Sci 40:1099–1120. https://doi.org/10.1016/j.ijrmms.2003.07.009

Vu TM, Sulem J, Subrin D, Monin N (2013) Semi-analytical solution for stresses and displacements in a tunnel excavated in transversely isotropic formation with non-linear behavior. Rock Mech Rock Eng 46:213–229. https://doi.org/10.1007/s00603-012-0296-0

Wang TT, Huang TH (2009) A constitutive model for the deformation of a rock mass containing sets of ubiquitous joints. Int J Rock Mech Min Sci 46:521–530

Wang TT, Huang TH (2014) Anisotropic deformation of a circular tunnel excavated in a rock mass containing sets of ubiquitous joints: theory analysis and numerical modeling. Rock Mech Rock Eng 47:643–657. https://doi.org/10.1007/s00603-013-0405-8

Wang MB, Wang G (2013) A modified stress-displacement solution for a pressure tunnel with a permeable liner in an elastic porous medium based on a new model. Rock Mech Rock Eng 46:259–268. https://doi.org/10.1007/s00603-012-0283-5

Wang SY, Sloan SW, Tang CA, Zhu WC (2012) Numerical simulation of the failure mechanism of circular tunnels in transversely isotropic rock masses. Tunn Undergr Sp Technol 32:231–244. https://doi.org/10.1016/j.tust.2012.07.003

Wittke W (1990) Rock mechanics: theory and applications with case histories. Springer, Berlin

Wittke W (2014) Rock mechanics based on an anisotropic jointed rock model (AJRM). Wiley Blackwell, Berlin

Wu Q, Kulatilake PHSW (2012) Application of equivalent continuum and discontinuum stress analyses in three-dimensions to investigate stability of a rock tunnel in a dam site in China. Comput Geotech 46:48–68. https://doi.org/10.1016/j.compgeo.2012.05.013

Zareifard MR, Fahimifar A (2016) Analytical solutions for the stresses and deformations of deep tunnels in an elastic-brittle-plastic rock mass considering the damaged zone. Tunn Undergr Sp Technol 58:186–196. https://doi.org/10.1016/j.tust.2016.05.007

Zhang Z, Sun Y (2011) Analytical solution for a deep tunnel with arbitrary cross section in a transversely isotropic rock mass. Int J Rock Mech Min Sci 48:1359–1363. https://doi.org/10.1016/j.ijrmms.2011.10.001

Zhang ZX, Xu Y, Kulatilake PHSW, Huang X (2012) Physical model test and numerical analysis on the behavior of stratified rock masses during underground excavation. Int J Rock Mech Min Sci 49:134–147. https://doi.org/10.1016/j.ijrmms.2011.11.001